


# Structural, Optical, and Magnetic Properties of Solution-Processed Co-Doped ZnS Thin Films

A. GOKTAS <sup>1,2,4,5</sup> and İ.H. MUTLU<sup>3</sup>

1.—Department of Physics, Faculty of Arts and Sciences, Harran University, 63300 Sanliurfa, Turkey. 2.—Department of Physics and Materials, Interdisciplinary Faculty of Science and Engineering, Shimane University, Matsue 690-8504, Japan. 3.—Department of Materials Science and Engineering, Akdeniz University, 07058 Antalya, Turkey. 4.—e-mail: agoktas@harran.edu.tr. 5.—e-mail: agoktas63@gmail.com

Co-doped ZnS thin films have been grown on glass substrates using solution-processing and dip-coating techniques, and the impact of the Co doping level (0% to 5%) and film thickness on certain characteristics examined. X-ray diffraction study revealed that all the films possessed hexagonal crystal structure. Energy-dispersive x-ray analysis confirmed presence of Zn, Co, and S in the samples. Scanning electron microscopy showed that the film surface was homogeneous and dense with some cracks and spots. X-ray photoelectron spectroscopy confirmed introduction and integration of  $\text{Co}^{2+}$  ions into the ZnS thin films. Compared with undoped ZnS, optical studies indicated a reduction in optical bandgap energy ( $E_g$ ) while the refractive index ( $n$ ), extinction coefficient ( $k$ ), and dielectric constants ( $\epsilon_1$ ,  $\epsilon_2$ ) increased with film thickness ( $t$ ) and Co doping level (except for 5%). Photoluminescence spectra showed enhanced luminescence intensity as the Co concentration was increased, while the dependence on  $t$  showed an initial increase followed by a decrease. The origin of the observed low-temperature (5 K and 100 K) ferromagnetic order may be related to point defects such as zinc vacancies, zinc interstitials, and sulfide vacancies or to the grain-boundary effect.

**Key words:** Co-doped ZnS, solution processing, photoluminescence, refractive index, dielectric constant, paramagnetic/ferromagnetic behavior

## INTRODUCTION

Doped semiconductor thin films have been extensively studied in recent years due to their outstanding characteristics and application potential.<sup>1–4</sup> Doping or quantum confinement of carriers is one of the key features that make such materials unique, being an effective way to tune their properties. In particular, transition-metal-doped dilute magnetic semiconductors (DMSs) have attracted enormous attention because of their widespread use in laser, nonlinear optical, electroluminescent, photoluminescent, spintronic, and quantum devices.<sup>5–8</sup> Doping of transition-metal impurities such as Mn,

Fe, and Co into wide-band semiconductors is one way to achieve DMS materials.

Recently, among all II–IV-based DMS materials, zinc sulfide (ZnS) doped with transition-metal ions<sup>3,9–13</sup> has been extensively studied as an attractive material. This is due to its nontoxic nature, high efficiency, cost-effectiveness, good transparency in the visible range, high exciton binding energy (40 meV), wide bandgap [3.61 eV in the cubic zincblende (ZB) structure,<sup>2</sup> 3.77 eV for hexagonal wurtzite (WZ) structure],<sup>14</sup> and superior optical properties,<sup>15</sup> permitting the combination of magnetic, photonic, and electronic characteristics in one material.

It is well known that nanostructured and polycrystalline ZnS thin films play an important role in the solar cell and optoelectronic areas. Such films can also be used as buffer layers in several types of

thin-film solar cell.<sup>16,17</sup> Higher conversion efficiency of 17.4% is achieved in Cu(In,Ga)(SSe) thin-film photovoltaics.<sup>18</sup> The structural, optical, and magnetic properties of ZnS can be modulated via variation of its size, chemical composition, and impurity doping.<sup>1,2,19,20</sup>

Due to its attractive and unique properties, ZnS might be an indispensable host semiconductor material for DMS applications. Accordingly, doping ZnS with various metals such as Mn, Cu, and Co has received much attention, opening the possibility of manufacturing a variety of optoelectronic and magneto-optic devices; For instance, Polat et al.<sup>19</sup> reported that the metal doping concentration may change the microstructure as well as the optical and magnetic properties of Co-doped zinc oxysulfide thin films. Inamdar et al.<sup>20</sup> demonstrated that the bandgap of ZnS(O) thin films can be tuned by using different transition metals such as Mn, Ni, and Co. Patel et al.<sup>3</sup> reported the magnetic properties of  $Zn_{1-x}Co_xS$  thin films, observing paramagnetic or ferromagnetic order depending on the sintering temperature and Co doping ratio.

Many researchers have reported different characteristics of diverse transition-metal-doped ZnS nanoparticles.<sup>1,21–25</sup> It is reported that  $Co^{2+}$  ( $r_{Co^{2+}} = 0.058$  nm)<sup>26</sup> and  $Zn^{2+}$  ions ( $r_{Zn^{2+}} = 0.060$  nm) have approximately the same ionic radius and that  $Co^{2+}$  could be incorporated at ZnS lattice sites by substitution for  $Zn^{2+}$  up to 15 at.% to 20 at.%<sup>27</sup> without destroying the structure.  $Co^{2+}$  has also been selected as a good magnetic candidate due to its comparatively large magnetic response, making Co-doped nanostructured ZnS an ideal candidate for investigation of its structural, optical, and magnetic characteristics.

So far, for investigation of their structural, optical, and magnetic properties, Co-doped ZnS/Zn(O,S) thin films have been produced by the pulsed laser deposition (PLD) technique<sup>3</sup> or spray pyrolysis method.<sup>19</sup> However, the Co-doped Zn(O,S) thin films resulting from the spray pyrolysis method, which include not only sulfur but also oxygen, are not an array Co-doped ZnS system. There is little or no research on solution-processed pure Co-doped ZnS obtained by dip-coating, especially in thin-film form.<sup>3,34</sup> Among proposed techniques to produce Co-doped ZnS thin films, solution processing (sometimes called the sol-gel process) is the most popular because of its relatively low cost and facile production of metal-doped ZnS thin films.<sup>35,36</sup>

Therefore, the aim of this study is to produce the first solution-processed Co-doped ZnS thin films by dip-coating and to investigate the impact of the Co doping ratio and thickness ( $t$ ) on their structural, optical, and magnetic properties.

## EXPERIMENTAL PROCEDURES

### Synthesis of Co-Doped ZnS System

Co-doped ZnS thin films with various Co doping levels (0%, 1%, 3%, and 5%) were grown on glass

substrates using the solution-based dip-coating technique. To obtain the Co-doped ZnS compounds, reactants zinc acetate [ $Zn(CH_3COO)_2 \cdot 2H_2O$ , 99.99 at.% purity], cobalt nitrate [ $Co(NO_3)_2 \cdot 6H_2O$ , 99.98 at.% purity], and thiourea [ $SC(NH_2)_2$ , 99 at.% purity] were used. Methanol and triethanolamine were also used as solvent and stabilizer, respectively. Zinc acetate (0.1 M) and the appropriate amount of cobalt nitrate were dissolved in 20 ml methanol and stirred for 30 min. Separately prepared 0.3 M thiourea solution was added dropwise to this mixture. The pH of the total mixture was regulated to 7.8 using triethanolamine. The final solution was mixed at 300 K under continuous magnetic stirring (250 rpm) for 3 h to obtain the desired solution.

After deposition, the films were instantly dried at 573 K in a vertically located furnace under air environment, then the dried films were instantly annealed in a horizontal quartz tube furnace at 873 K (heating rate 0.2°C/s) under Ar environment for 15 min. To obtain films with the desired  $t$ , the above dip-coating process was repeated 15 times.

### Characterization Techniques

The structural properties of the Co-doped ZnS thin films were studied using high-resolution x-ray diffraction (XRD) analysis (Rigaku Ultima III diffractometer, Cu  $K_\alpha$  radiation with  $\lambda = 0.15406$  nm,  $V = 40$  kV,  $I = 40$  mA). The film samples were scanned from 20° to 70° ( $2\theta$ ) in steps of 0.02°. Surface morphology and film thickness were observed by scanning electron microscopy (SEM, Zeiss Evo 50) using a Röntec 3000 detector at operating voltage of 15 kV. The  $t$  value of the samples was determined from SEM cross-sectional micrographs to be 520 nm, 640 nm, 635 nm, and 600 nm for ZnS thin films with 0%, 1%, 3%, and 5% Co, respectively. Optical absorption spectra were observed using a PerkinElmer 45 dual-beam ultraviolet–visible (UV–Vis) spectrophotometer in the wavelength range from 300 nm to 900 nm.

The presence of elements in the films was confirmed by energy-dispersive x-ray spectroscopy (EDX) at 30 kV and x-ray photoelectron spectroscopy (XPS) at scanning rate of 1 eV. The chemical composition and bonding types present on the surface and in the near-surface region of the films were investigated by XPS using a Thermo monochromated high-performance XPS spectrometer system (PHI-5000 Versa probe) equipped with an Al  $K_\alpha$  x-ray radiation source at energy of 1486.6 eV. Photoluminescence (PL) spectra of the Co-doped ZnS films were obtained at room temperature using a Hitachi F-2500 FL spectrophotometer. Magnetic measurements were carried out using a superconducting quantum interference device (SQUID) magnetometer (Quantum Design, MPMS-XL) at temperatures ranging from 5 K to 300 K.

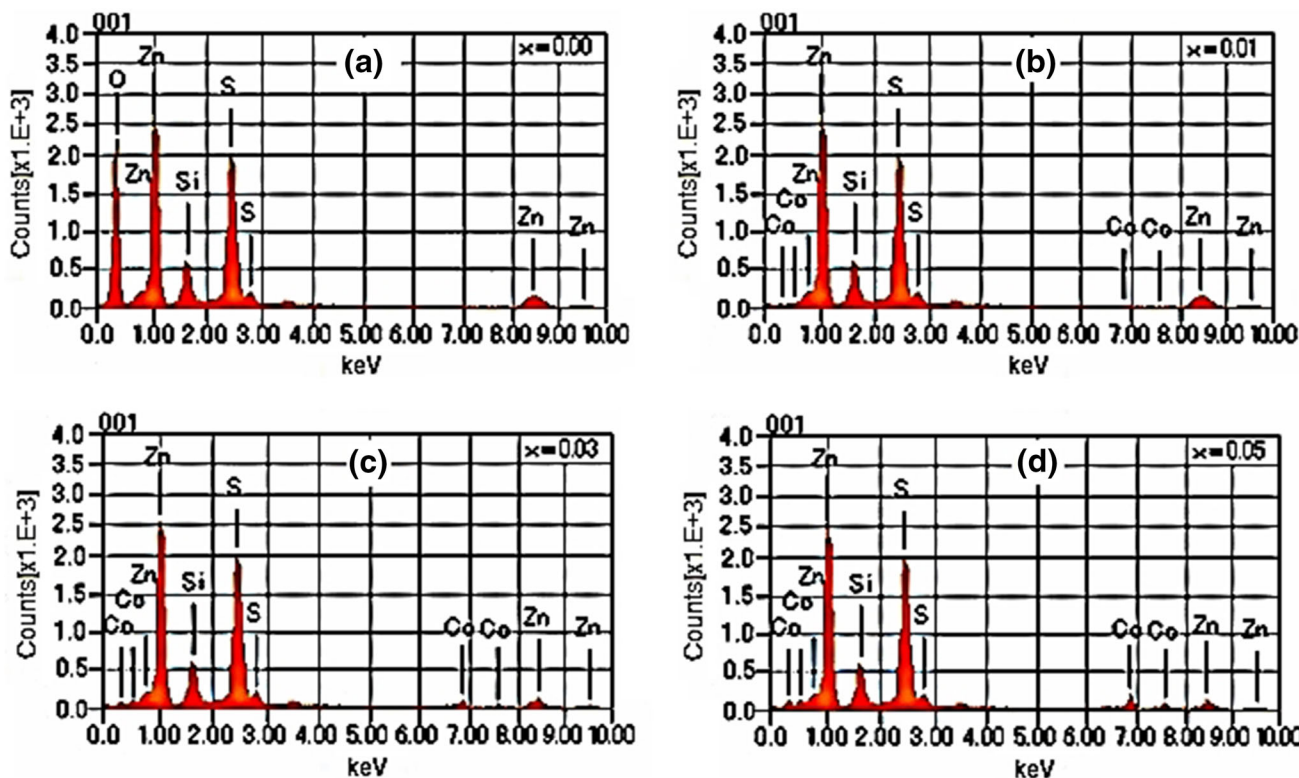


Fig 1. EDX spectra of undoped ZnS (a), 1% Co-doped ZnS (b), 3% Co-doped ZnS (c), and 5% Co-doped ZnS (d) thin films deposited on glass substrate.

## RESULTS AND DISCUSSION

### Chemical Analysis

Figure 1 shows the EDX spectra for the ZnS and Co-doped ZnS thin films. The spectra exhibits presence of Zn, Si, O, Co, and S elements in the films. However, for the undoped sample, only Zn, Si, O, and S elements were found, with no Co signal observed. The presence of Si and O signals is probably due to the glass substrate.<sup>27,35,36</sup> The EDX peak intensity of Co dopant increased with increasing Co doping ratio, in good agreement with the estimated chemical composition of the films, as shown in Table I. Hence, only the chemical composition is discussed below.

To confirm the chemical binding states in the Co-doped ZnS thin films, the near-surface chemical nature of the films was determined by XPS measurements. Figure 2 shows a typical XPS spectrum (for the 3% Co-doped ZnS thin film annealed at 873 K), recorded in the binding energy range from 0 eV to 1200 eV. The spectrum shows various peaks, corresponding to Zn, S, Co, C, O, and Na elements. These observed peaks were also reported in Ref. 22. Furthermore, the other peaks related to C 1s and O 1s might have resulted from surface contamination. Additionally, researchers have previously observed peaks corresponding to Zn 3s, 3p, 3d, Co 2s, O KLL, Co LMM, and Zn LMM.<sup>19,27,28</sup>

The XPS signals related to Zn, Co, and S are shown for a Co-doped ZnS composition in Fig. 2. In the wide-scan XPS spectrum, two signals at 1020 eV and 1043 eV (Fig. 3a) can be ascribed to  $Zn^{2+}$ , matching well with the binding energy of Zn–S bond.<sup>29</sup> The peaks located around 160 eV and 171 eV correspond to S 2p bonding (Fig. 3b), which might be because of Zn–S bonds and surface impurities, respectively.<sup>30</sup> The obtained results are in agreement with reported values.<sup>19,20</sup> The presence of Co is proved by the Co 2p<sub>3/2</sub> and Co 2p<sub>1/2</sub> signals shown in Fig. 3c at corresponding binding energy of 781 eV and 796 eV, suggesting incorporation of Co<sup>2+</sup> in the ZnS films. The binding energy of the Co 2p<sub>3/2</sub> and Co 2p<sub>1/2</sub> signals do not match with the corresponding energy of Co metal at 777.9 eV and 792.95 eV. This indicates that Co<sup>2+</sup> dopant is certainly diffused into the ZnS.<sup>31,32</sup> The observed values for Co are consistent with values reported in Ref. 19.

### Morphological Studies

SEM micrographs of the ZnS and Co-doped ZnS samples are shown in Fig. 4. It can be seen that the morphology of the samples is smooth, homogeneous, and dense with some cracks and spots, and the surface grains are uniformly distributed (Fig. 4). Spots were also observed previously on ZnS thin

**Table I. SEM elemental composition analysis of undoped and Co-doped ZnS thin films fabricated on glass substrate**

| Co Doping level (%) | Chemical composition                    | Zn Content (%) | Co content (%) | S content (%) | Total (%) | Spectrum line |
|---------------------|---|----------------|----------------|---------------|-----------|---------------|
| 0                   | ZnS                                     | 50.38          |                | 49.62         | 100       | K             |
| 1                   | Zn <sub>0.99</sub> Co <sub>0.01</sub> S | 49.56          | 1.03           | 49.44         | 100       | K             |
| 3                   | Zn <sub>0.98</sub> Co <sub>0.03</sub> S | 47.72          | 2.96           | 49.32         | 100       | K             |
| 5                   | Zn <sub>0.97</sub> Co <sub>0.05</sub> S | 46.70          | 4.89           | 48.41         | 100       | K             |

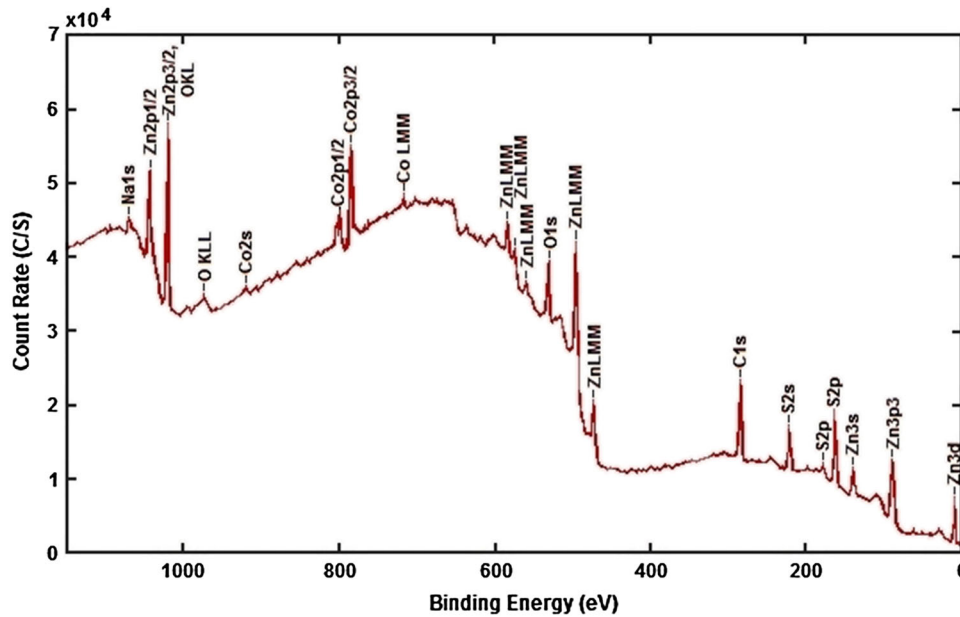


Fig 2. XPS spectrum of Co-doped ZnS thin film deposited on glass substrate.

films.<sup>2</sup> The actual grain size of the Co-doped ZnS samples could not be clearly determined from SEM images due to the limited resolution of the SEM instrument. The grain size of the Co-doped ZnS films increases first with increase of Co concentration. However, it later decreases monotonically depending on the *t*. A similar change was also observed for the crystallite size of the Co-doped ZnS thin films (Table II).

### Structural Studies

The crystalline phase and crystallite size of the Co-doped ZnS thin films were determined by XRD analysis as given in Fig. 5. The results of the XRD studies demonstrated that the films had polycrystalline nature. For all the films, the observed (100), (002), (101), and (112) plane signals were in good agreement with Joint Committee on Powder Diffraction Standards (JCPDS) card no. 01-36-1450. Accordingly, the diffraction patterns of the films indicated hexagonal WZ-type ZnS structure with strong preferred orientation along hexagonal

(002) plane direction. This result is consistent with previous studies showing hexagonal WZ structure with preferred orientation along hexagonal (002) plane direction for Co-doped Zn(O,S) thin films prepared by the spray pyrolysis method,<sup>19</sup> electron-beam evaporated ZnS:Mn,<sup>33</sup> and sol-gel derived Fe- and Mn-doped ZnS thin films.<sup>34,35</sup> However, cubic ZB structure with preferred crystallographic orientation along (111) plane was reported for Co-doped ZnS nanoparticles by Poornaprakash et al.<sup>1</sup> and Akhtar et al.<sup>36</sup>

For all the films, it is clear that the (002) diffraction peak is stronger and narrower than the other peaks, suggesting preferential growth along *c*-axis direction. No diffraction peaks for any Co compounds (sulfides, oxides, etc.) or other impurity phases were detected for the films. These results indicate that Co may have merely entered into the ZnS lattice but did not undergo any chemical reactions with sulfur to form new compounds. The full-width at half-maximum (FWHM) of the (002) peak decreased with increasing Co doping concentration, indicating improved crystalline quality of

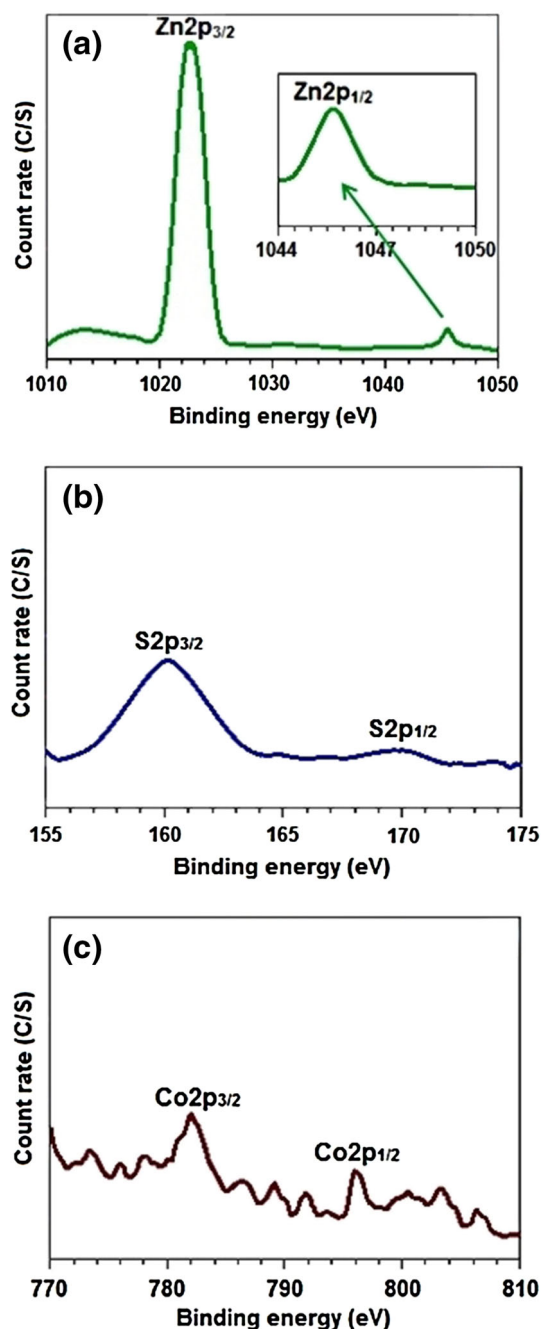


Fig 3. Wide-scan XPS spectrum of 3% Co-doped ZnS thin film for (a) Zn, (b) S, and (c) Co.

the Co-doped ZnS thin films. This is supported by the grain size of the films as given in Fig. 4, which shows that the grain size of the Co-doped ZnS films was larger than that of the undoped ZnS thin film.

The average crystallite size of the films was calculated using the Debye–Scherrer equation ( $D = k\lambda/\beta\cos\theta$ ), first increasing with the Co doping content but then decreasing monotonically for further increase (Table II). As seen from Table II, the average crystallite size of the Co-doped ZnS thin films increased for 1% Co doping with higher  $t$  but

decreased monotonically for higher Co doping ratios with decreasing film  $t$ . This shows that  $t$  contributes to the improvement in crystalline quality of the films. In previous study on Co-doped ZnS nanospheres, an increase in average crystallite size of the samples was reported.<sup>37</sup> However, the crystallite size of chemically precipitated Co-doped ZnS nanoparticles decreased with increasing Co concentration, as reported by Pathak et al.<sup>21</sup> Furthermore, there are no studies on the effect of Co concentration and  $t$  on the crystallite size of Co-doped ZnS thin films for comparison. The different results for the crystallite size of Co-doped ZnS samples might be due to the different preparation techniques and conditions applied.

The lattice parameter ( $c$ ) of the samples was calculated from the position of the highest intensity of the ZnS (002) peak using the standard relation for a hexagonal system. The dependence of the  $c$  parameter on the Co concentration of the Co-doped ZnS thin films is presented in Table II. It is obvious that  $c$  changes from 0.6252 nm to 0.6230 nm with increasing Co doping concentration from 0% to 5%. There is no important shift in  $c$  with increasing Co doping ratio, which might be due to the substitution of  $Zn^{2+}$  ions ( $r_{Zn^{2+}} = 0.060$  nm) with  $Co^{2+}$  ions ( $r_{Co^{2+}} = 0.058$  nm<sup>19,27</sup>). In addition, the shift in  $c$  may depend on the uniform stress and the combination of contaminant atoms with different ionic radii in the lattice, which leads to a change in stoichiometry, etc. Hence, the shift of the  $c$  parameter found in this study is caused by various effects, resulting in a net decrease in the  $c$  value.

### Optical Studies

The optical properties of the ZnS and Co-doped ZnS thin films were investigated in the wavelength range from 300 nm to 900 nm. The optical absorption spectra of the undoped and Co-doped ZnS samples are shown in Fig. 6. To obtain the absorption spectra of the films alone, the contribution of the glass substrate was subtracted. A sharp absorption edge between wavelength of 320 nm and 380 nm was observed for all samples (Fig. 6). With increasing Co dopant level, redshift of the absorption edge was found, being maximum for the 3% Co dopant concentration. This is attributed to introduction of Co atoms at low concentration into the ZnS lattice.<sup>38</sup> As the Co doping level is increased,  $sp-d$  interaction<sup>7</sup> may lead to blueshift of the absorption edge.

The absorption bumps at wavelength of 670 nm, 710 nm, and 732 nm can be attributed to substitution of  $Co^{2+}$  ions at tetrahedral  $Zn^{2+}$  sites, likely being due to transitions from  ${}^4A_2(F)$  to  ${}^2F(G)$ ,  ${}^4A_2(F)$  to  ${}^4T_2(P)$ , and  ${}^4A_2(F)$  to  ${}^4A_1(G)$  levels,<sup>3,39,40</sup> indicating integration of  $Co^{2+}$  at  $Zn^{2+}$  tetrahedral sites in ZnS.

The fundamental absorption, which corresponds to electron excitation from valence to conduction

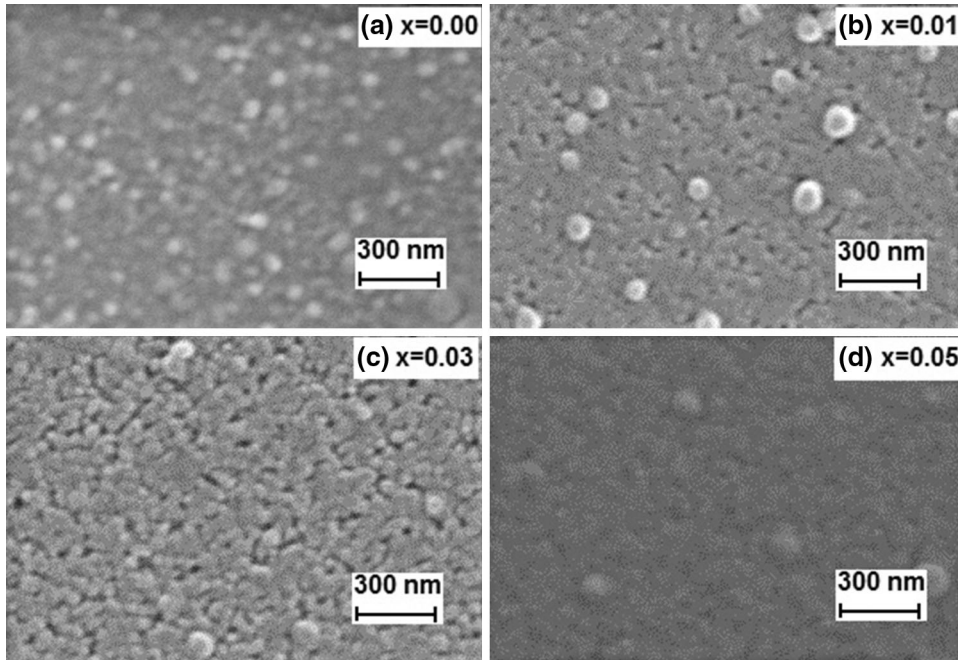


Fig 4. SEM images of undoped ZnS (a), 1% Co-doped ZnS (b), 3% Co-doped ZnS (c), and 5% Co-doped ZnS (d) thin films deposited on glass substrate.

**Table II. Selected structural and optical parameters, obtained by XRD and UV-Vis analyses, for Co-doped ZnS thin films fabricated on glass substrate**

| Co Doping Level (%) | FWHM, $\beta$ ( $^{\circ}$ ) | $2\theta$ ( $^{\circ}$ ) | Crystallite Size (nm) | $c$ (nm) | $t$ (nm) | $E_g$ (eV) |
|---------------------|------------------------------|--------------------------|-----------------------|----------|----------|------------|
| 0                   | 1.16                         | 28.52                    | 7                     | 0.6252   | 520      | 3.60       |
| 1                   | 0.40                         | 28.52                    | 13                    | 0.6252   | 640      | 2.84       |
| 3                   | 0.32                         | 28.44                    | 12                    | 0.6269   | 635      | 2.87       |
| 5                   | 0.24                         | 28.62                    | 10                    | 0.6230   | 600      | 3.04       |

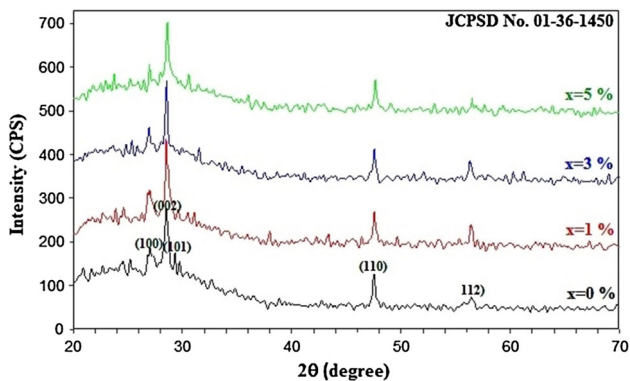


Fig 5. XRD patterns of Co-doped ZnS thin films deposited on glass substrate.

band, can be used to determine the  $E_g$  value of all the synthesized thin films. The  $E_g$  of the presented films was determined using the Tauc relation,<sup>41-43</sup>

$$\alpha h\nu = C(h\nu - E_g)^n, \quad (1)$$

where  $C$  is a constant and  $n$  is also a constant associated with different types of electronic transition ( $n = 1/2, 2, 3/2$  or  $3$  for direct allowed, indirect allowed, direct forbidden, and indirect forbidden transitions, respectively).

The optical  $E_g$  values were found to be 3.60 eV, 2.84 eV, 2.87 eV, and 3.04 eV for the 0%, 1%, 3%, and 5% Co-doped ZnS thin films, respectively (Fig. 7). These values are lower than the value for bulk ZnS (3.68 eV for ZB and 3.91 eV for WZ phase) due to defect states, which produce absorption tailing.

It is clear that the  $E_g$  value initially decreased sharply on 1% Co doping, then increased monotonically with increasing Co doping concentration. The reduction of  $E_g$  might be because of the following reasons: (1) the  $sp-d$  interaction<sup>34,44</sup> between band electrons and localized  $d$  electrons of  $\text{Co}^{2+}$  and  $\text{Zn}^{2+}$ , resulting in a decrement of  $E_g$ ; (2) the nanoscale

effect; (3) the level of impurities; (4) and parameters related to the structure. Recently, similar behavior was reported in  $Zn_{1-x}Mn_xS$  and  $Zn_{1-x}Co_xO$  thin films synthesized by sol-gel dip- and spin-coating methods, respectively.<sup>34,44</sup> As reported in Ref. 3, a decrease in  $E_g$  for  $Zn_{1-x}Co_xS$  thin films deposited by the PLD technique has also been observed.

As seen in Table II, compared with undoped ZnS, the  $E_g$  value initially decreased with increasing  $t$  for

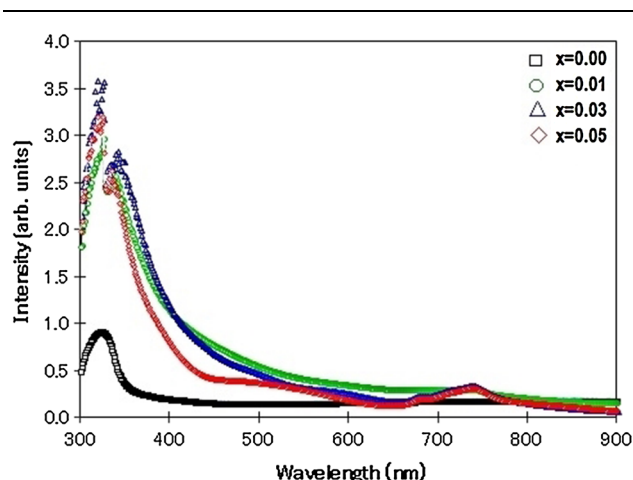


Fig 6. Optical absorption spectra of Co-doped ZnS thin films deposited on glass substrate.

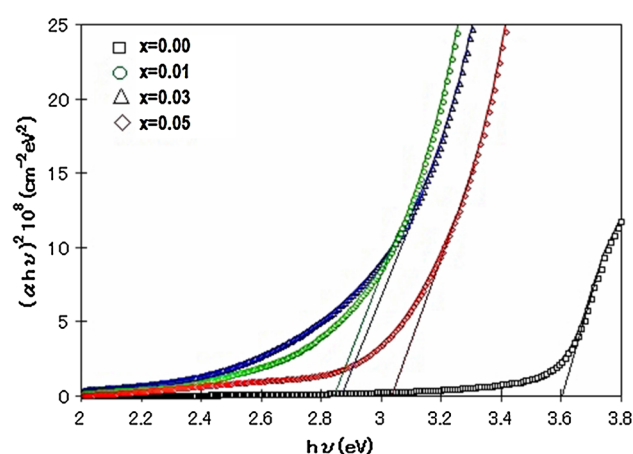


Fig 7. Calculation of optical bandgap from optical absorption spectra for Co-doped ZnS thin films deposited on glass substrate.

the lowest doping ratio of Co (1%), then increased monotonically with decreasing  $t$  for higher Co concentrations. This can be attributed to the fact that, in case of thicker films, more atoms are present, so more states are available for photon absorption. The change in  $E_g$  with the  $t$  value of the Co-doped ZnS films can be understood based on the quantum size effect observed in nanocrystalline thin films. In this way, the redshift for the Co-doped ZnS films can be attributed to the Co doping concentration,  $t$ , and average crystallite size of the films. A similar redshift of  $E_g$  for films of higher  $t$  and/or average crystallite size was reported for  $Zn_{1-x}Mn_xS$  and  $Zn_{1-x}Mn_xO$  nanocrystalline thin films with pH value of 7.5.<sup>4,34</sup>

The  $n$  value for a semiconductor can be determined from  $E_g$ <sup>46</sup> values using Eq. 2:

$$\frac{n^2 - 1}{n^2 + 1} = 1 - \left(\frac{E_g}{20}\right)^{1/2}. \quad (2)$$

Compared with undoped ZnS, the obtained  $n$  values initially increased on Co doping and then gradually decreased for higher Co doping levels, as presented in Table III. This is probably related to modification of the polarizability of ions and the local field within ZnS due to Co doping. The  $k$  value of the fabricated films was also calculated using the absorption coefficient via Eq. 3:

$$k = \frac{\alpha\lambda}{4\pi}, \quad (3)$$

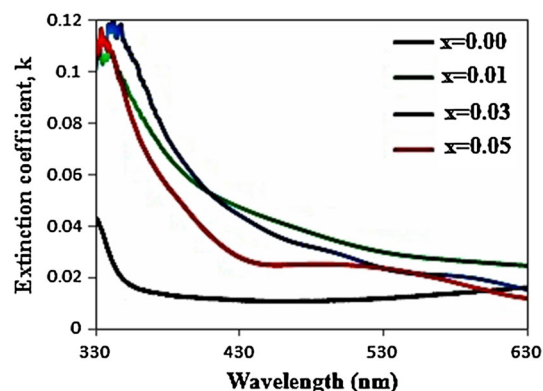


Fig 8. Extinction coefficient versus wavelength for 1%, 3%, and 5% Co-doped ZnS thin films.

**Table III. Selected optical and dielectric constants as functions of film thickness and Co doping level for Co-doped ZnS thin films**

| Co Doping Level (%) | Film Thickness, $t$ (nm) | $E_g$ (eV) | $n$   | $k$   | $\epsilon_1$ | $\epsilon_2$ |
|---------------------|--------------------------|------------|-------|-------|--------------|--------------|
| 0                   | 520                      | 3.60       | 1.925 | 0.024 | 3.705        | 0.092        |
| 1                   | 640                      | 2.84       | 2.075 | 0.046 | 4.303        | 0.190        |
| 3                   | 635                      | 2.87       | 2.068 | 0.044 | 4.274        | 0.181        |
| 5                   | 600                      | 3.04       | 2.034 | 0.037 | 4.145        | 0.150        |

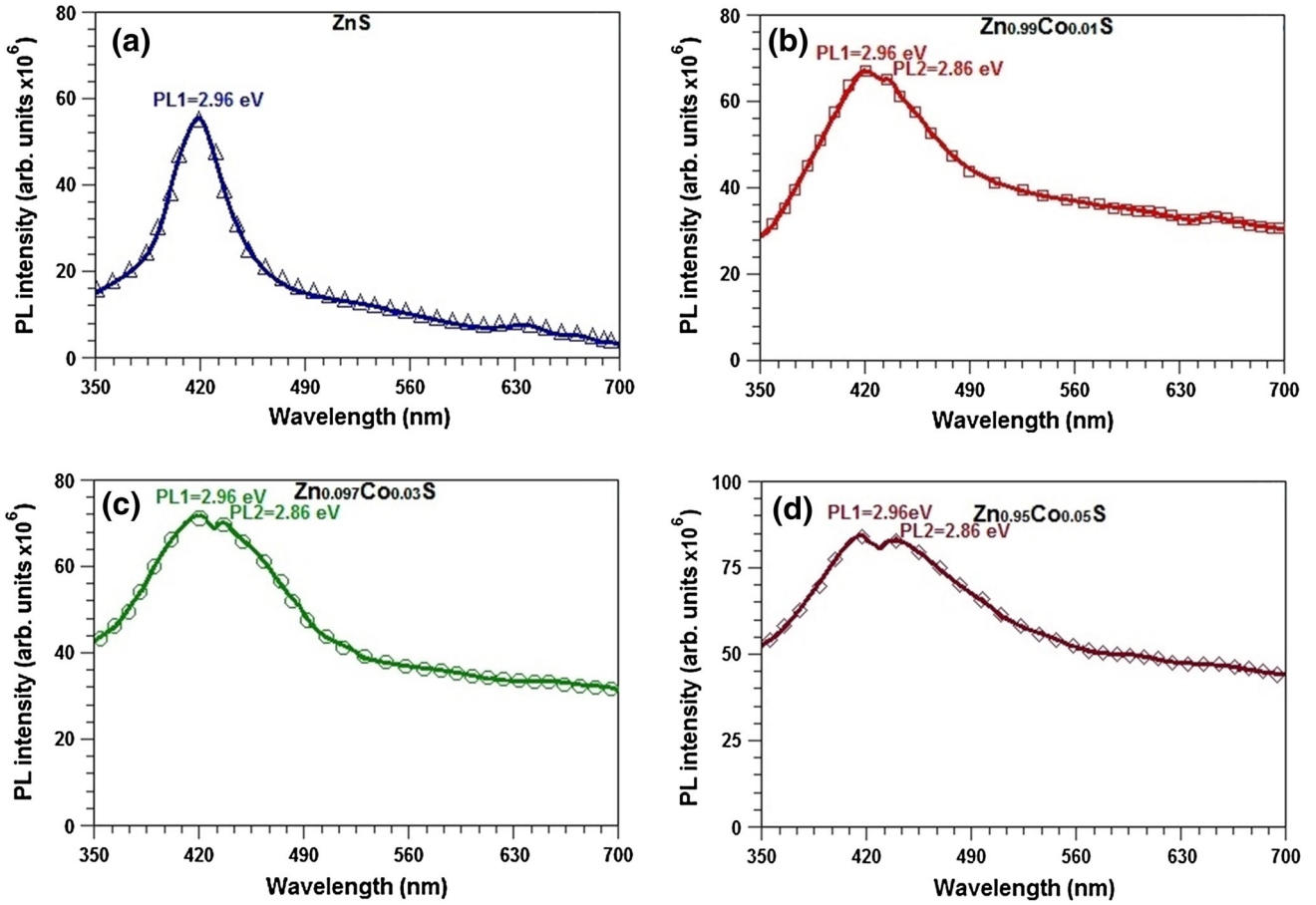


Fig 9. PL spectra of Co-doped ZnS thin films for different Co contents: (a) 0%, (b) 1%, (c) 3%, and (d) 5%.

where  $\alpha$  is the absorption coefficient, which is related to the absorbance and  $t$ , and  $\lambda$  is the incident photon wavelength. Plots of  $k$  versus  $\lambda$  are shown in Fig. 8, indicating a sharp decrease in the wavelength range from 330 nm to 430 nm then a monotonic reduction in the visible range. Note that the  $k$  values for the Co-doped ZnS thin films were higher than that for undoped ZnS thin film. The  $k$  value obtained at a wavelength corresponding to the  $E_g$  value of each film is given in Table III. Compared with undoped ZnS, both  $k$  and  $n$  values increased with increasing  $t$  and decreasing  $E_g$ , except for the 5% Co doping level.

The optical dielectric constant of a material is composed of real ( $\epsilon_1$ ) and imaginary ( $\epsilon_2$ ) parts, both of which can be calculated at the wavelength corresponding to  $E_g$  by using Eqs. 4 and 5:

$$\epsilon_1 = n^2 - k^2, \quad (4)$$

$$\epsilon_2 = 2nk. \quad (5)$$

As seen from Table III, the  $\epsilon_1$  values of the films were higher than their  $\epsilon_2$  values. It was found that the  $\epsilon_1$  and  $\epsilon_2$  values of the films increased with  $t$  and the Co doping concentration (except for 5%). Among

all the fabricated films, the highest  $n$ ,  $k$ ,  $\epsilon_1$ , and  $\epsilon_2$  values were found for the 1% Co-doped ZnS thin films.

### Photoluminescence Studies

PL spectra of the ZnS and Co-doped ZnS thin films were recorded using an excitation wavelength of 344 nm at room temperature. As seen in Fig. 9a, the observed PL peak at 418 nm (PL1) is likely related to surface defects (as also obviously evident from the XPS results) of the ZnS thin films. It is clear that the observed PL1 peak had energy lower than the  $E_g$  value (3.60 eV) of the ZnS thin films. This finding is well consistent with results for Zn(S,O) thin films prepared by the chemical bath deposition (CBD) technique,<sup>20</sup> where the observed peak was also attributed to surface defect states of the Zn(S,O) thin films.

For the Co-doped ZnS samples, an additional blue emission peak (PL2) was observed at around 433 nm (Fig. 9b–d). The corresponding energy related to this PL2 blue emission is also lower than that of the band-edge emission of the ZnS thin films, likely being attributable to surface defects.<sup>1,20</sup> With increasing Co doping concentration and increasing/decreasing  $t$ , no change in the blue emission



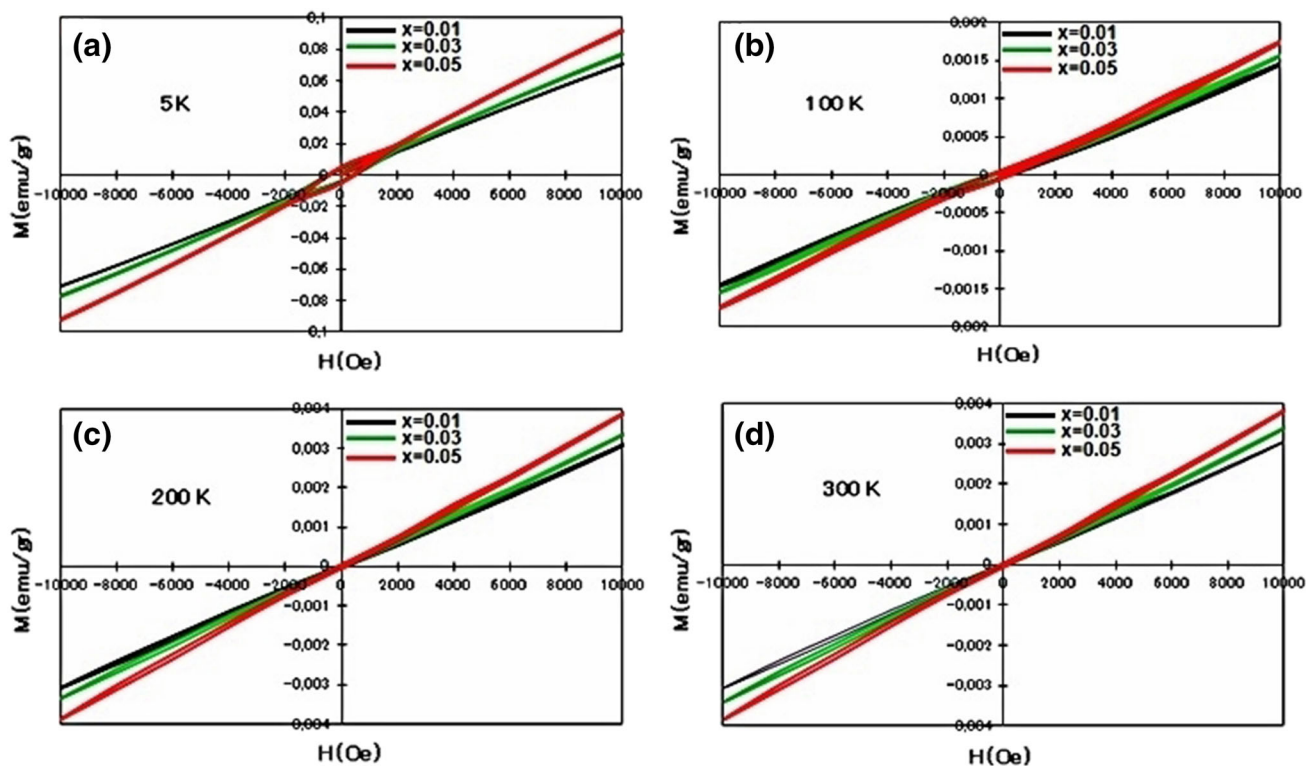


Fig. 10.  $M$ - $H$  curves of Co-doped ZnS thin films at temperature of 5 K (a), 100 K (b), 200 K (c), and 300 K (d).

wavelength was observed (Fig. 9a–d). Moreover, it is very interesting that use of an appropriate Co doping ratio in the ZnS host could significantly increase the PL intensity of the thin film. This can be attributed to the substitution of newly added Co atoms at Zn sites to form Co-doped ZnS, which could lead to fewer interstitial S atoms and Zn vacancies in the lattice of the ZnS host. This finding may be correlated with the XRD data, as it can be seen from Table II that the FWHM of the (002) plane reflection for the Co-doped ZnS samples was lower than that for undoped ZnS, revealing an increase in particle size for the Co-doped ZnS thin films. Similar results with increasing PL intensity for higher Co dopant concentration have also been reported for Co-doped ZnS nanoparticles.<sup>15,21,25,37</sup>

### Magnetic Properties

Curves of magnetization ( $M$ ) as a function of applied magnetic field,  $M(H)$ , recorded at 5 K, 100 K, 200 K, and 300 K for the Co-doped ZnS thin films, are shown in Fig. 10. The diamagnetic or paramagnetic component from the glass substrate was given in our previous study,<sup>34</sup> allowing its subtraction from all data. It was found that the samples exhibited ferromagnetic behavior at 5 K and 100 K but paramagnetic behavior at 200 K and 300 K for the Co-doped ZnS thin films.

These observed trends differ from those in earlier reports on the Co-doped ZnS system; For example,

Vatankhah et al.<sup>44</sup> found superparamagnetic behavior at low temperatures (2 K to 10 K) in nanocrystalline  $Zn_{1-x}Co_xS$  synthesized by a wet chemical method, and ferromagnetic response was reported at room temperature for Co-doped Zn(O,S) thin films prepared by the spray pyrolysis method at 673 K.<sup>19</sup> Recently, the magnetic properties of  $Zn_{1-x}Co_xS$  ( $x = 0.025$  and  $0.05$ ) thin films deposited by the PLD technique at different annealing temperatures ( $T_A$ ) of 473 K, 673 K, and 873 K were reported. The magnetic response of the paramagnetic and ferromagnetic components in these samples depended on  $T_A$  and the Co concentration. More recently, room-temperature ferromagnetism was reported in Co-doped ZnS thin films<sup>36</sup> and nanoparticles.<sup>1</sup> However, the observed ferromagnetic behavior at 5 K and 100 K is in agreement with the reported magnetic response of  $Zn_{1-x}Co_xS$  ( $x = 0.025$ ) thin films,<sup>3</sup> which showed ferromagnetic behavior at low temperatures, and also with the ferromagnetic behavior observed at 20 K for Co-doped Zn(O,S) thin films.<sup>19</sup>

The above-mentioned results confirm that the film preparation technique and conditions such as the annealing environment and temperature, gaseous pressure of the annealing environment, and starting chemicals used to obtain the Co-doped ZnS system are the main factors resulting in different magnetic behavior.

As seen from Fig. 11a and b, the Co-doped ZnS thin films exhibited a clear hysteresis loop at 5 K

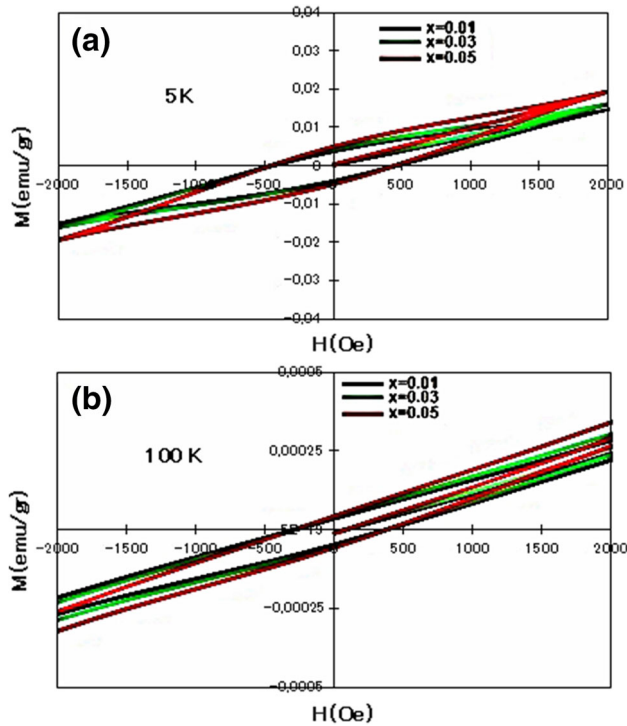


Fig. 11.  $M$ - $H$  curves of Co-doped ZnS thin films at 5 K (a) and 100 K (b).

and 100 K in the low magnetic field region (0 Oe to 2000 Oe), indicating that the ferromagnetic response at 5 K (Fig. 11a) was stronger than that at 100 K (Fig. 11b). It can also be seen from Fig. 11a and b that the coercive field, remanent  $M$ , and saturation  $M$  values for the samples increased with increasing Co doping concentration and decreasing  $t$ , reflecting increased magnetic interactions at low temperatures. Consistent with the results observed at low magnetic field ( $H < 2000$  Oe), ferromagnetic behavior was also reported for  $Zn_{1-x}Co_xS$  ( $x < 0.06$ ) nanoparticles.<sup>45</sup>

To explain the complex magnetic behavior of our films, temperature-dependent magnetization  $M(T)$  measurements were performed under magnetic field of 500 Oe and temperatures ranging from 5 K to 300 K (Fig. 12). As seen in Fig. 12, the  $M$  value of the Co-doped ZnS thin films exhibited a slow increase with decreasing temperature from 300 K to 35 K, followed by an abrupt increase upon further cooling. This behavior reflects the paramagnetic response.  $M$  increased as the dopant ratio was increased and  $t$  decreased, reflecting the paramagnetic nature as also observed in the  $M(H)$  curves. This finding is in agreement with the result reported (in the high temperature region of 10 K to 300 K) for nanocrystalline  $Zn_{1-x}Co_xS$  prepared under  $N_2$  environment at room temperature.<sup>46</sup>

The observed ferromagnetic behavior at 5 K and 100 K is probably due to diffusion of Co into the ZnS lattice, giving rise to cobalt-related impurity phases and Co clusters not observed by XRD or XPS

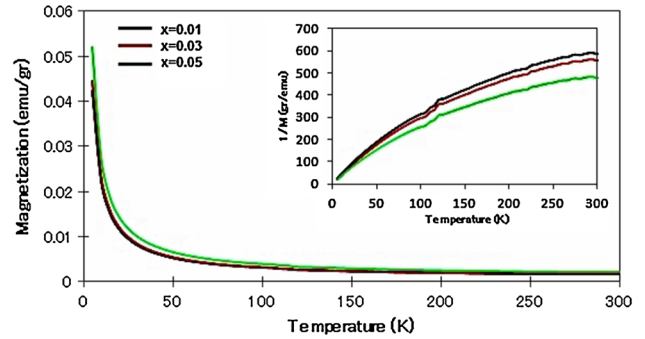


Fig. 12. Temperature dependence of magnetization for Co-doped ZnS thin films deposited on glass substrate; inset:  $M^{-1}$  versus  $T$  curves of Co-doped ZnS thin films.

measurements.<sup>47</sup> This suggests that the ferromagnetic behavior is not due to Co-related secondary phases. Nonetheless, it has been suggested that presence of transition-metal-related impurities cannot be observed by XRD or XPS when the doping ratio is 5% in the Ni- or Fe-doped ZnO system.<sup>48</sup> It has been reported that point defects related to zinc and sulfur can significantly affect the ferromagnetic characteristics of transition-metal-doped ZnS dilute magnetic semiconductors.<sup>30,34</sup> This may be one reason for the observed low-temperature ferromagnetism in the present samples. Moreover, Patel et al.<sup>3</sup> suggested that the ferromagnetic response of Co-doped ZnS could be strongly affected by grain boundaries, being the other reason for the observed low-temperature ferromagnetism of the solution-processed Co-doped ZnS thin films. Finally, the observed low-temperature ferromagnetism is probably also due to point defects such as zinc vacancies, zinc interstitials, and sulfur vacancies, as also evidenced by PL and XPS studies.<sup>33,38</sup>

The inset of Fig. 12 shows the inverse of the magnetization for the films as a function of temperature; the plot of  $M^{-1}$  versus  $T$  directly shows proportional behavior from 5 K to 300 K, suggesting paramagnetic behavior of the Co-doped ZnS thin films. The observed results were investigated using the Curie-Weiss equation,

$$\chi = C/(T + \theta), \quad (6)$$

where  $\chi$  is the magnetic susceptibility,  $C$  is the paramagnetic Curie constant, and  $\theta$  is the Curie-Weiss temperature. The Curie-Weiss temperature for the samples having 1%, 3%, and 5% Co was close to zero ( $-18$  to  $-34$ ), as obtained by extrapolating the high-temperature linear part of the  $1/M$  versus  $T$  curves to  $1/M = 0$  (Fig. 12). The observed Curie-Weiss temperatures reveal weak antiferromagnetic interaction between the Co magnetic moments, leading to paramagnetic behavior. However, for bulk  $Zn_{1-x}Co_xS$ , large negative Curie-Weiss temperatures ( $-50$  K to  $-100$  K) were reported, indicating strong antiferromagnetic interaction.<sup>49,50</sup>

Finally, our results are in good agreement with previous studies on Co-doped ZnS/Zn(S,O) thin films or nanoparticles and make important additional contributions. Additionally, the solution-processing and dip-coating techniques have various advantages over techniques previously applied for the  $\text{Zn}_{1-x}\text{Co}_x(\text{S},\text{O})$  system,<sup>3,19</sup> due to the following reasons: (1)  $\text{Zn}_{1-x}\text{Co}_x(\text{S},\text{O})$  thin films fabricated by the spray pyrolysis method contain oxygen and not just the  $\text{Zn}_{1-x}\text{Co}_x\text{S}$  system, whereas the present films are the raw  $\text{Zn}_{1-x}\text{Co}_x\text{S}$  system; (2) the other method proposed for the Co-doped ZnS system is the PLD technique,<sup>3</sup> which needs high-vacuum conditions for film deposition and is not convenient for production of large-area films compared with solution-processing techniques; (3) furthermore, the solution-processing and dip-coating techniques are comparatively ordinary and affordable compared with the PLD technique; (4) moreover, the good compatibility of these first solution-processed, dip-coated Co-doped ZnS samples in thin-film form may result in wide applications in the areas of spintronic and optoelectronic devices. We believe that this study makes crucial contributions to the literature in terms of both techniques and findings for the Co-doped ZnS thin-film system.

## CONCLUSIONS

Co-doped ZnS thin films were synthesized by a solution-processing and dip-coating method for the first time. XRD analysis revealed a polycrystalline hexagonal wurtzite-type crystalline structure for the ZnS and Co-doped ZnS films. A remarkable change in film morphology and grain size was observed on changing the Co dopant concentration and  $t$  value. Presence of Zn, Co, and S was confirmed by EDX and XPS measurements. Integration of  $\text{Co}^{2+}$  ions with  $\text{Zn}^{2+}$  ions in the ZnS host lattice was evidenced by XRD, XPS, EDX, and optical absorption analyses. It was found that the optical  $E_g$  initially reduced then increased on varying both  $t$  and the Co dopant level. With increasing Co doping level, the  $n$ ,  $k$ ,  $\varepsilon_1$ , and  $\varepsilon_2$  values of the films increased in comparison with the ZnS host, except for the 5% Co doping level. It was also found that the PL intensity and low-temperature ferromagnetic response of the films might be tunable by adjusting the doping concentration and  $t$  value.

## ACKNOWLEDGEMENTS

This work was supported by the Scientific and Technological Research Council of Harran University (HUBAK) with Project No. 15029. The authors are grateful to Prof. Dr. Yasuji Yamada and Dr. Funaki Shuhei, Department of Physics and Materials, Interdisciplinary Faculty of Science and Engineering, Shimane University, Japan, for the use of laboratory instruments, hosting and guiding one of the authors (A.G.) during his fellowship at Shimane University.

## REFERENCES

- B. Poornaprakash, D. Amaranatha Reddy, G. Murali, N. Madhusudhana Rao, R.P. Vijayalakshmi, and B.K. Reddy, *J. Alloy. Compd.* 577, 79 (2013).
- A. Goktas, F. Aslan, E. Yasar, and I.H. Mutlu, *J. Mater. Sci.: Mater. Electron.* 23, 1361 (2012).
- S.P. Patel, J.C. Pivin, A.K. Chawla, R. Chandra, D. Kanjilal, and L. Kumar, *J. Magn. Magn. Mater.* 323, 2734 (2011).
- A. Goktas, I.H. Mutlu, Y. Yamada, and E. Celik, *J. Alloy. Compd.* 553, 259 (2013).
- N. Kumbhojkar, V.V. Nikesh, A. Kshirsagar, and S. Mahamuni, *J. Appl. Phys.* 88, 6260 (2000).
- N. Goswami and P. Sen, *J. Nanopart. Res.* 9, 513 (2007).
- A. Goktas, I.H. Mutlu, and Y. Yamada, *Superlatt. Microstruct.* 57, 139 (2013).
- T. Dietl, H. Ohno, F. Matsukura, J. Cibert, and D. Ferrand, *Science* 287, 1019 (2000).
- J. Xie, *J. Magn. Magn. Mater.* 322, L37 (2010).
- Y. Li, Z. Zhou, P. Jin, Y. Chen, S.B. Zhang, and Z. Chen, *J. Phys. Chem. C* 114, 12099 (2010).
- S. Sambasivam, D.P. Joseph, J.G. Lin, and C. Venkateswaran, *J. Solid State Chem.* 182, 2598 (2009).
- G. Ren, Z. Lin, C. Wang, W. Liu, J. Zhang, F. Huang, and J. Liang, *Nanotechnology* 18, 035705 (2007).
- K. Sato and H. Katayama-Yoshida, *Phys. Status Solidi B* 229, 673 (2002).
- H.C. Ong and R.P.H. Chang, *Appl. Phys. Lett.* 79, 3612 (2001).
- R. Sarkar, C.S. Tiwary, P. Kumbhakar, and A.K. Mitra, *Physica B* 404, 3855 (2009).
- S.D. Sartale, B.R. Sankapal, M. Lux-Steiner, and A. Ennaoui, *Thin Solid Films* 480, 168 (2005).
- A. Ennaoui, W. Eisele, M. Lux-Steiner, T.P. Niesen, and F. Karg, *Thin Solid Films* 431, 335 (2003).
- R.N. Bhattacharya and K. Rammanathan, *Sol. Energy* 77, 679 (2004).
- I. Polat, S. Aksu, M. Altunbaş, and E. Bacaksız, *Mater. Chem. Phys.* 130, 800 (2011).
- A.I. Inamdar, S. Lee, D. Kim, K.V. Gurav, J.H. Kim, H. Im, W. Jung, and H. Kim, *Thin Solid Films* 537, 36 (2013).
- C.S. Pathak, M.K. Mandal, and V. Agarwala, *Mater. Sci. Semicond. Process.* 16, 467 (2013).
- N. Karar and H. Chander, *J. Nanosci. Nanotechnol.* 5, 1498 (2005).
- R.N. Bhargava, D. Gallager, X. Hong, and A. Nurmikko, *Phys. Rev. Lett.* 72, 416 (1994).
- Nie Eryong, Liu Donglai, Zhang Yunsen, Bai Xue, Yi Liang, Jin Yong, Jiao Zhifeng, and Sun Xiaosong, *Appl. Surf. Sci.* 257, 8762 (2011).
- P. Yang, M. LuE, D. XuE, D. Yuana, C. Songa, and G. Zhou, *J. Phys. Chem. Solids* 62, 1181 (2001).
- R.D. Shannon, *Acta Crystallogr. A* 32, 751 (1976).
- A. Goktas, F. Aslan, and I.H. Mutlu, *J. Alloy. Compd.* 615, 765 (2014).
- L. Wei, Z. Li, and W.F. Zhang, *Appl. Surf. Sci.* 255, 4992 (2009).
- S.W. Shin, S.R. Kang, J.H. Yun, A.V. Moholkar, J.H. Moon, J.Y. Lee, and J.H. Kim, *Sol. Energy Mater. Sol. Cells* 95, 856 (2011).
- W.S. Ni, Y.J. Lin, C.J. Liu, Y.W. Yang, and L. Horng, *J. Alloy. Compd.* 556, 178 (2013).
- B.J. Tan, K.J. Klabunde, and P.M.A. Sherwood, *J. Am. Chem. Soc.* 113, 855 (1991).
- Y. Okamoto, T. Imanaka, and S. Teranishi, *J. Catal.* 65, 448 (1980).
- M. El-Hagary, M. Emam-Ismael, E.R. Shaaban, A. Al-Rashidi, and S. Althoyaib, *Mater. Chem. Phys.* 132, 581 (2012).
- A. Goktas, I.H. Mutlu, and J. Sol-Gel, *Sci. Technol.* 69, 120 (2014).
- A. Goktas, *Appl. Surf. Sci.* 340, 151 (2015).
- M.S. Akhtar, Y.G. Alghamdi, M.A. Malik, R.M.A. Khalil, S. Riaz, and S. Naseemb, *J. Mater. Chem. C* 3, 6755 (2015).

37. L.-J. Tang, G.-F. Huang, Y. Tian, W.-Q. Huang, M.-G. Xia, C. Jiao, J.-P. Long, and S.-Q. Zhan, *Mater. Lett.* 100, 237 (2013).
38. X. Ma and Z. Wang, *Microelectron. Eng.* 88, 3168 (2011).
39. J. Dreyhsig, K. Klein, H.-E. Gumlich, and J.W. Allen, *Solid State Commun.* 85, 19 (1994).
40. P. Koidl, *Phys. Rev. B* 15, 2492 (1977).
41. T. Badapanda, S.K. Rout, L.S. Cavalcante, J.C. Sczancoski, S. Panigrahi, E. Longo, and M. Siu Li, *J. Phys. D Appl. Phys.* 42, 175414 (2009).
42. S. Singh and P. Chakrabarti, *Adv. Sci. Eng. Med.* 5, 677 (2013).
43. S. Vyas, P. Giri, S. Singh, and P. Chakrabarti, *J. Electron. Mater.* 44, 3401 (2015).
44. F.L. Xian, L.H. Xu, X.X. Wang, and X.Y. Li, *Cryst. Res. Technol.* 47, 423 (2012).
45. J. Bian, X. Li, L. Chen, and Q. Yao, *Chem. Phys. Lett.* 393, 256 (2004).
46. C. Vatankhah, S. Jafargholinejad, S. Karami, and R. Vatankhah, *Aust. J. Basic Appl. Sci.* 4, 4423 (2010).
47. M.T. Le and J. Lee, *Geosyst. Eng.* 16, 231 (2013).
48. P.H. Borse, N. Deshmukh, R.F. Shinde, S.K. Date, and S.K. Kulakarni, *J. Mater. Sci.* 34, 6087 (1999).
49. C.J. Chen, W. Gao, Z.F. Qin, W. Hu, and M. Qu, *J. Appl. Phys.* 70, 6277 (1991).
50. A. Lewicki, A.I. Schindler, J.K. Furdyna, and W. Giriat, *Phys. Rev. B* 40, 2379 (1989).